Journal of Solid State Chemistry 183 (2010) 590–594

Contents lists available at ScienceDirect

Journal of Solid State Chemistry

journal homepage: www.elsevier.com/locate/jssc

One-dimensional organic photoconductive nanoribbons built on Zn–Schiff base complex

Li Liu [a,b], Ming-Wang Shao [a,c,*], Xiu-Hua Wang [a]

[a] Anhui Key Laboratory of Functional Molecular Solids, College of Chemistry and Materials Science, Anhui Normal University, Wuhu 241000, PR China
[b] Department of Biochemical Engineering, Anhui University of Technology and Science, Wuhu 241000, PR China
[c] Functional Nano and Soft Materials Laboratory (FUNSOM), Soochow University, Suzhou 215123, PR China

ARTICLE INFO

Article history:
Received 17 September 2009
Received in revised form
25 December 2009
Accepted 1 January 2010
Available online 11 January 2010

Keywords:
Schiff base zinc
Organic nanoribbons
Photoluminescence
Photoconductivity

ABSTRACT

One-dimensional organic nanoribbons built on *N*-*p*-nitrophenylsalicylaldimine zinc complex were synthesized via a facile solvothermal route. The scanning electron microscope images revealed that the as-synthesized products were ribbon-like with width mainly of 300–600 nm, thickness of about 50 nm, and length of up to tens of micrometers. Fourier transform infrared spectrum was employed to characterize the structure. Ultraviolet–visible absorption and photoluminescence spectra showed that the products had good photoluminescent property and exhibited blue emission. The conductivity of a bundle of nanoribbons was also measured, which showed that the Schiff base zinc nanoribbons had good photoconductive property. This work might enrich the organic photoconductive materials and be applicable in light-controlled micro-devices or nano-devices in the future.

1. Introduction

Nanomaterials based on traditional functional organic molecules have emerged as promising and prospective next-generation materials owing to the variety, multifunctionality, designability, and tailorability [1–5]. Since the efficient low-voltage-driven organic light-emitting diodes based on tris(8-hydroxyquinoline) aluminium (AlQ_3) were first reported in 1987 [6], organometallic complexes have particularly attracted a lot of attentions in organic photoluminescent material regions [7].

One-dimensional (1D) organic nanomaterials are more suitable for the construction of active nanodevices and interconnects compared with nanomaterials with other morphology [5]. However, most of the approaches to 1D inorganic nanomaterials are not applicable to organic nanomaterials because of their lower melting points and thermal instability. There are only a few successful preparations of 1D organic nanomaterials reported up to now, such as self-assembly of multifunctional molecules in solution [8–10], templates [3,11], vapor deposition technique [12].

Solvothermal synthesis is widely applied in preparation of 1D inorganic nanomaterials as a mild and feasible method [13]. It is available and significant to explore this method to prepare functional 1D organic nanomaterials [14,15]. Then, this method was employed here to prepare Schiff base zinc nanoribbons.

Schiff base metal complexes are promising materials for photoelectronic applications, and the easiness of synthesis allows structural modification for optimization of material properties [16–26]. Schiff base zinc complexes are particularly attractive for their interesting photoluminescent properties. The salicylideneamine–zinc(II) complexes exhibit photoluminescence as well as electroluminescence [16–23], and display strong blue photoluminescence both in solution and in the solid state [27].

In this report, *N*-*p*-nitrophenylsalicylaldimine zinc nanoribbons had been prepared and the photoconductive property was measured. The results showed good photoconductive property and might be found potential application in the fabrication of photosensor or nano-devices in the future.

2. Experimental

2.1. Materials

Salicylaldehyde was distilled under reduced pressure and *p*-nitrophenylamine was recrystallized from ethanol before used. Zinc acetate dihydrate ($ZnAc_2 \cdot 2H_2O$), ethanol and methanol of analytical grade chemicals were used without further treatment.

* Corresponding author at: Anhui Key Laboratory of Functional Molecular Solids, College of Chemistry and Materials Science, Anhui Normal University, Wuhu 241000, PR China. Fax: +86 553 3869303.
E-mail address: mwshao@mail.ahnu.edu.cn (M.-W. Shao).

0022-4596/$ - see front matter © 2010 Elsevier Inc. All rights reserved.
doi:10.1016/j.jssc.2010.01.003

2.2. Preparation of nanoribbons built on N-p-nitrophenylsalicylaldimine zinc

The reaction of equivalent salicylaldehyde and *p*-nitrophenylamine in ethanol under 90 °C for 2 h gave *N*-*p*-nitrophenylsalicylaldimine (Schiff base) ligand crude product. The Schiff base ligand was recrystallized from ethanol before used. In a typical synthesis of Schiff base zinc nanoribbons, 0.25 mmol $ZnAc_2\cdots 2H_2O$ and 0.5 mmol *N*-*p*-nitrophenylsalicylaldimine were dissolved into 40 mL methanol under stirring, which was transferred into a stainless 50 mL Teflon-lined autoclave, heated at 140 °C for 12 h and cooled to room temperature. Then ultrapure water was added dropwise into the resulting solution. After settled for about 12 h, the resulting yellowish flocculent suspension was separated centrifugally, washed with ultrapure water for several times, and then dried under vacuum at 60 °C for 10 h.

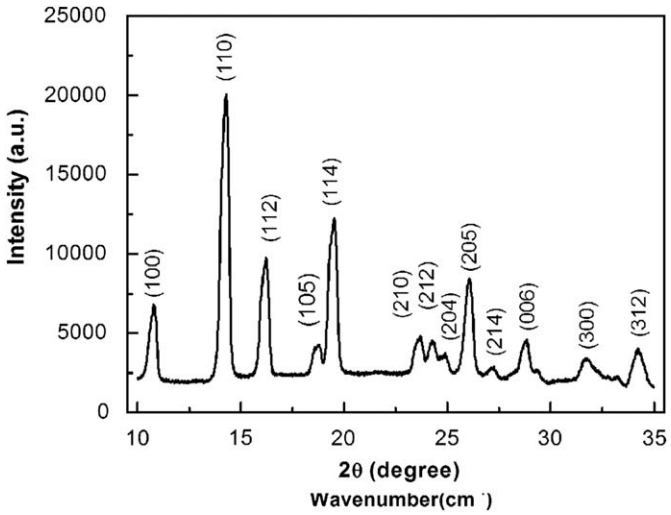

Fig. 1. XRD pattern of the products.

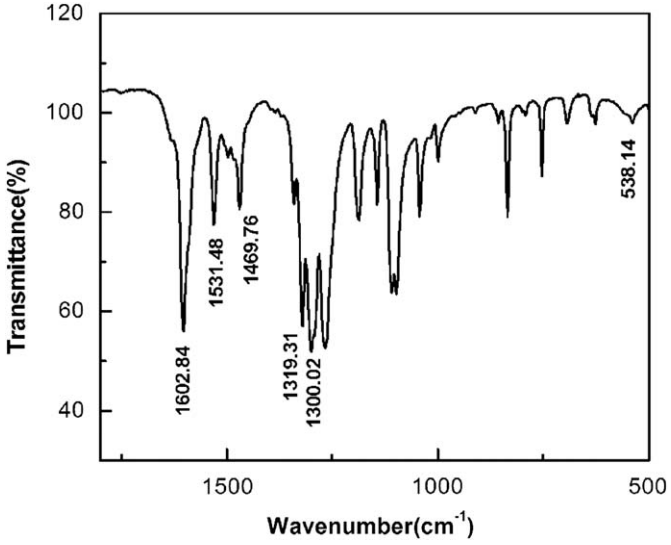

Fig. 2. FTIR spectrum of the products.

2.3. Characterization

The powder X-ray diffraction (XRD) pattern was recorded on X'Pert-Pro Materials Research Diffractometer equipped with Cu Kα radiation (λ=0.15406 nm); a scanning rate of 0.0167 °s^{-1} was applied to record the pattern in the 2θ range 10–35°. The morphology and size of the products were studied by a Hitachi S-4800 scanning electron microscope (SEM). Fourier transform infrared (FTIR) spectrum was obtained with KBr pellets for solids on a Shimadzu FTIR-8400S spectrometer. Ultraviolet–visible (UV–vis) absorption spectrum was recorded on a PerkinElmer Lambda 750 UV/vis spectrophotometer at room temperature. The photoluminescence excitation (PLE) and photoluminescence (PL) spectra of the as-prepared samples were measured using a fluorescence spectrophotometer Edinburgh FLS920 at room temperature. Thermogravimetric analysis–differential thermal analysis (TGA–DTA) measurement of the products was performed in SETARAM-TGA92 in the temperature range room temperature–500 °C at a heating rate of 10 °C min^{-1}. The electrical measurements were tracked with a CHI 620B electrochemical workstation. The low magnification image was taken from an Olympus optical microscope.

3. Results and discussion

Fig. 1 shows the XRD pattern of the *N*-*p*-nitrophenylsalicylaldimine zinc nanoribbons. The peaks at 2θ=10.78, 14.32, 16.19, 18.76, 19.53, 23.64, 24.26, 24.88, 26.05, 27.24, 28.84, 31.77, 34.22° show the as-prepared samples are crystalline in nature. This pattern was indexed as tetragonal phase with crystal constants a=0.8677 ± 0.0022 nm, and c=2.2723 ± 0.0127 nm, using the Hesse-Lipson method [28,29].

The FTIR spectrum is recorded to reveal the composition of products as shown in Fig. 2. The intense infrared stretch at 1602 cm^{-1} is assigned typically to the imine C=N bond, which makes a shift towards lower frequency compared to the ν(C=N) band in Schiff base ligand. It shows that in our products the nitrogen atom of the azomethine group takes part in the coordination [30]. The peak at 1319 cm^{-1} is assigned to the C–O

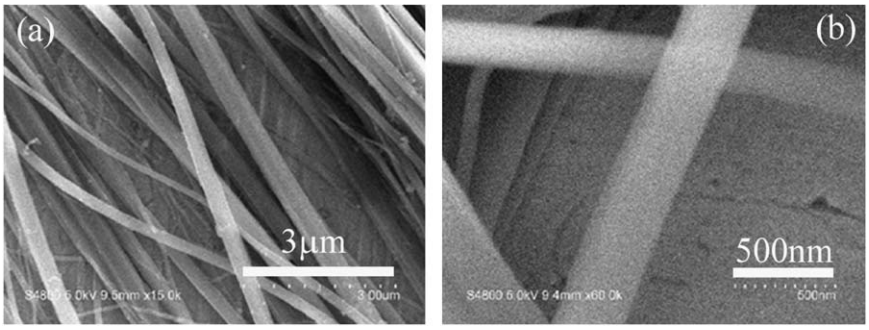

Fig. 3. SEM images of the products attained at 140 °C: (a) Low magnification; (b) high magnification.

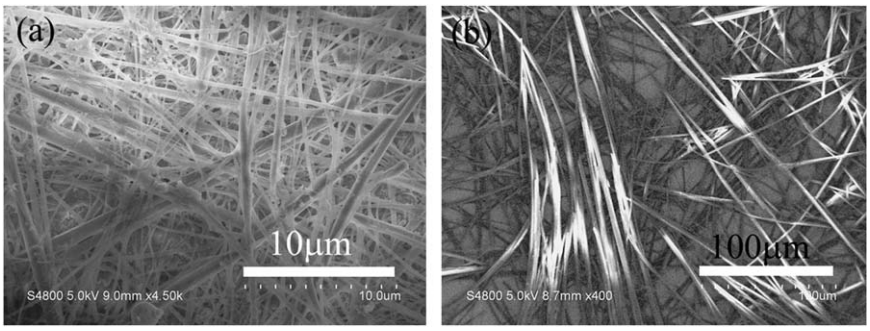

Fig. 4. SEM images of the products attained at reaction temperature higher than 140 °C: (a) 160 °C with low magnification; (b) 180 °C with low magnification.

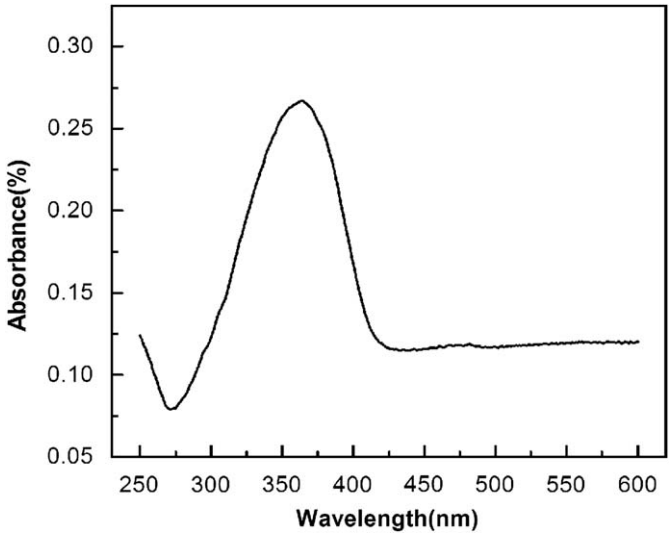

Fig. 5. UV–vis absorption spectrum of the products in solid state at room temperature.

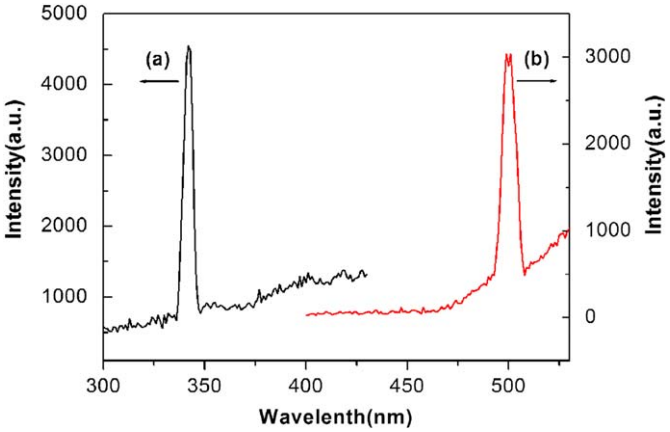

Fig. 6. Room temperature spectra of the products: (a) PLE spectrum with the emission of 500 nm; (b) PL spectrum excited at 342 nm.

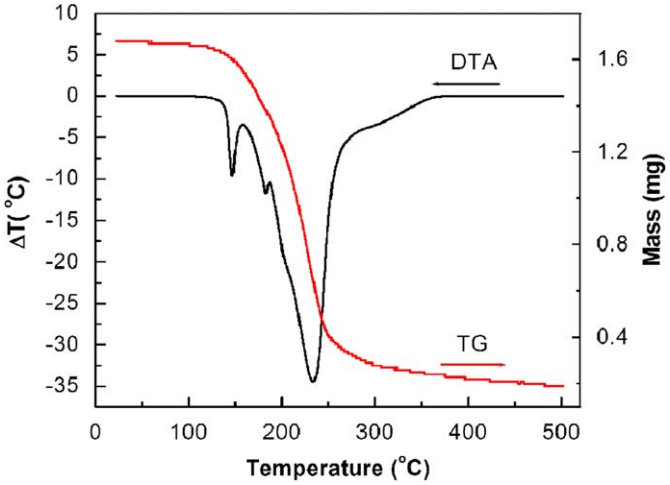

Fig. 7. TGA and DTA curves of the products.

stretching vibration, and the peak at 538 is attributed to Zn–O stretching vibrations. The symmetry stretching vibration peak of $-NO_2$ is at 1300 cm^{-1}. The feeble peak of Zn–N is not in the range of measurement. These vibrational modes are in good agreement with the previous report [31], which further supports that the as-prepared products are *N-p*-nitrophenylsalicylaldiminato zinc.

The SEM images (Figs. 3(a) and (b)) clearly reveal that the as-synthesized products are ribbon-like with width mainly of 300–600 nm, thickness of about 50 nm, and length of up to tens of micrometers.

In the growth process of Schiff base zinc nanoribbons, the solvent and temperature both influenced the morphology of the products. The selection of ethanol as the reaction solvent could not result in nanoribbons. When methanol was used as the reaction solvent, the SEM images of the Schiff base zinc nanoribbons attained at different reaction temperatures are shown in Figs. 3 and 4.

Large-scale Schiff base zinc nanoribbons could be obtained at the heating temperature of 140 °C (Figs. 3(a) and (b)), while no nanoribbons were formed below 120 °C. When the heating temperature was higher than 140 °C, such as 160 and 180 °C (Figs. 4(a) and (b)), the width of the obtained nanoribbons were about 1–2 μm.

Fig. 5 reveals the UV–vis absorption spectrum of Schiff base zinc nanoribbons in solid state at room temperature. In this spectrum, the maximum absorption peak was observed at a wavelength of 364 nm.

The PLE and PL spectra of Schiff base zinc nanoribbons at room temperature were acquired and shown in Fig. 6. The PLE spectrum (Fig. 6(a)) reveals that Schiff base zinc nanoribbons have an excitation peak at 342 nm under an emission of 500 nm. The PL spectrum excited at 342 nm (Fig. 6(b)) present a strong emission centered at 500 nm, which is an agreement with the related literature [27,32]. Both of the emission and excitation spectra are single-peak structure, which indicates the Schiff base zinc nanoribbons are uniform.

Fig. 7 displays TGA–DTA curves of Schiff base zinc nanoribbons heated from room temperature to 500 °C at a heating rate of

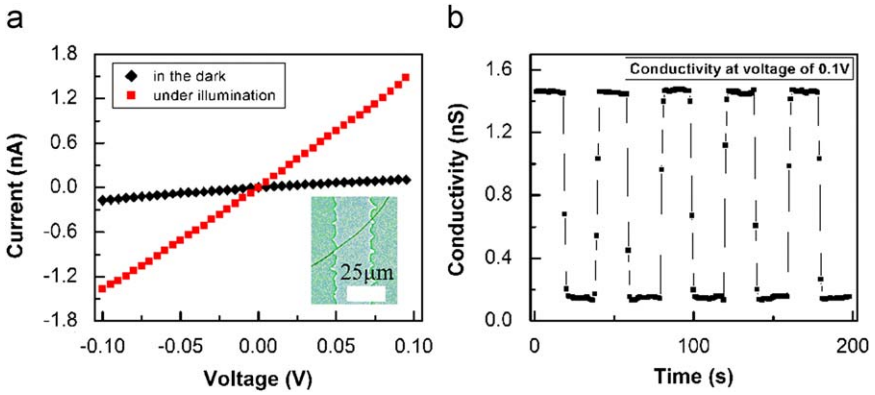

Fig. 8. (a) *I–V* curves of a bundle of the products measured (I) in a dark box (II) under illumination by using an incandescence lamp (12 V, 10 W); (b) photoconductive characteristics of the device during light switching on/off. A voltage of 0.1 V was applied across the Au–Au electrodes and the current was recorded during the light alternatively on and off at 20 s intervals.

$10\ ^{\circ}C\ min^{-1}$. The result shows the weight–loss temperature range 140–500 °C with the weight decreased from 1.68 to 0.19 g. The TG curve shows that there are three relatively feeble endothermic peaks at 146, 183 and 202 °C, which can represent the loss of water. A strong endothermic peak at 233 °C accounts for the loss of Schiff base ligands. After the products were thermally decomposed, the residue is ZnO. The total weight–loss ratio is determined as $(1.68-0.19)\div 1.68\times 100\%$. The calculation according to curves gives that one Zn(II) was coordinated by two Schiff base ligands in the samples and every product molecular contains 12 water molecules.

To measure the conductivity of the products, a bundle of Schiff base zinc nanoribbons were dispersed on an indium tin oxide (ITO) coated glass with an electrode gap of 25 μm. To increase injection of the device, Au gap electrodes were fabricated on the substrate by thermal evaporation with a micrometer-sized Au wire as the mask; by slightly moving the Au-wire mask, Au–Au gap electrodes were deposited. Then the conductivity was measured in a dark box or under illuminated by using an incandescence lamp (12 V, 10 W). In order to decrease the thermal effect, the power of the incandescence lamp was only 10 W and the distance of the device-to-light source was 10 cm. Fig. 8(a) shows the *I–V* curves measured in the dark or under illumination. The approximately linear shape of the curves reveals a good ohmic contact of the bundle of nanoribbons with the Au electrodes. It is clearly observed that the conductivity of the Schiff base zinc nanoribbons under illuminated increase evidently and enhances by 10 times, which might be found potential application in photoswitch nanodevices.

Fig. 8(b) shows the photoconductive characteristics of the device during light switching on/off. A voltage of 0.1 V was applied across the Au–Au electrodes and the current was recorded during the light alternatively on and off at 20 s intervals. The result shows the Schiff base zinc nanoribbons have good sensitivity to the light source switched on/off, which might find application in photosensitive nanodevices in the future.

The photoconductive property is size dependent [2] and is not possessed by matrix materials, which can be explained from the effect of the quantum effect. When the materials' size reduced to nano dimension, as a result of quantum confinement, the continuous energy levels split into discrete energy levels. Therefore, the external conduction sub-band and valence sub-band move in opposite directions to open up a band gap and correspondingly the effective band gap will be widened. In this particular material, the carrier mobility is also suppressed by carrier confinement along the long axis of the nanoribbon and by surface imperfection. Under illumination, the energy from the light excites the electrons in the semiconductor nanoribbons jumping from the valence band into the conduction band, leaving holes in valence band, increasing the charge carrier concentration via direct electron–hole pair creation and thus enhancing the current of the nanoribbons. Since the valence band energy levels in nanomaterials are lower than those in matrix materials, the current of the nanoribbions will be enhanced by more times under illumination. Then the nanomaterials have better photoconductivity.

4. Conclusions

The Schiff base zinc nanoribbons through a facile solvothermal route was successfully prepared in large scale, which showed good photoluminescent and photoconductive properties. This work might be applied in novel organic semiconductive or photoconductive nanodevices.

Acknowledgements

The project was supported by the National Natural Foundation of China (20571001) and College Natural Science Foundation of Anhui Province (KJ2009B003Z)

References

[1] Y.B. Wang, H.B. Fu, A.D. Peng, Y.S. Zhao, J.S. Ma, Y. Ma, J.N. Yao, Chem. Commun. (2007) 1623–1625.
[2] X.J. Zhang, J.S. Jie, W.F. Zhang, C.Y. Zhang, L.B. Luo, Z.H. He, X.H. Zhang, W.J. Zhang, C.S. Lee, S.T. Lee, Adv. Mater. 20 (2008) 2427–2432.
[3] J.S. Hu, Y.G. Guo, H.P. Liang, L.J. Wan, L. Jiang, J. Am. Chem. Soc. 127 (2005) 17090–17095.
[4] T.Q. Nguyen, R. Martel, P. Avouris, M. Bushey, C. Nuckolls, L.E. Brus, J. Am. Chem. Soc. 126 (2004) 5234–5442.
[5] Y.S. Zhao, H.B. Fu, A.D. Peng, Y. Ma, D.B. Xiao, J.N. Yao, Adv. Mater. 20 (2008) 2859–2876.
[6] C.W. Tang, S.A. VanSlyke, Appl. Phys. Lett. 51 (1987) 913–915.
[7] S. Wang, Coord. Chem. Rev. 215 (2001) 79–98.
[8] X.J. Zhang, X.H. Zhang, K. Zou, C.S. Lee, S.T. Lee, J. Am. Chem. Soc. 129 (2007) 3527–3532.
[9] B.-K. An, D.-S. Lee, J.-S. Lee, Y.-S. Park, H.-S. Song, S.Y. Park, J. Am. Chem. Soc. 126 (2004) 10232–10233.
[10] Y.S. Zhao, W. Yang, J. Yao, Phys. Chem. Chem. Phys. 8 (2006) 3300–3303.
[11] L. Zhao, W. Yang, Y. Luo, T. Zhai, G. Zhang, J. Yao, Chem. Eur. J. 11 (2005) 3773–3778.
[12] Y.S. Zhao, D.B. Xiao, W.S. Yang, A.D. Peng, J.N. Yao, Chem. Mater. 18 (2006) 2302–2306.
[13] F.X. Wang, M.W. Shao, L. Cheng, J. Hua, X.W. Wei, Mater. Res. Bull. 44 (2009) 1687–1691.

[14] Y.J. Chen, X.D. Chen, B.J. Li, D.S. Yu, Z.Q. He, G.J. Li, M.Q. Zhang, Appl. Phys. Lett. 89 (2006) 241121–241123.
[15] X.H. Wang, M.W. Shao, G. Shao, S.W. Wang, J. Nanosci. Nanotechnol. 9 (2009) 4709–4714.
[16] H. Kunkely, A. Vogler, Inorg. Chim. Acta 321 (2001) 171–174.
[17] Y.Z. Shen, H.W. Gu, Y. Pan, G. Dong, T. Wu, X.P. Jin, X.Y. Huang, H.W. Hu, J. Organomet. Chem. 605 (2000) 234–238.
[18] J. Qiao, L.D. Wang, L. Duan, Y. Li, D.Q. Zhang, Y. Qiu, Inorg. Chem. 43 (2004) 5096–5102.
[19] K.H. Chang, C.C. Huang, Y.H. Liu, Y.H. Hu, P.T. Chou, Y.C. Lin, Dalton Trans. (2004) 1731–1738.
[20] P.F. Wang, Z.R. Hong, Z.Y. Xie, S.W. Tong, O.Y. Wong, C.S. Lee, N.B. Wong, L.S. Hung, S.T. Lee, Chem. Commun. (2003) 1664–1665.
[21] Y. Hamada, T. Sano, M. Fujita, T. Fujii, Y. Nishio, K. Shibata, Jpn. J. Appl. Phys. 32 (1993) L511–L513.
[22] T. Sano, Y. Nishio, Y. Hamada, H. Takahashi, T. Usuki, K. Shibata, J. Mater. Chem. 10 (2000) 157–161.
[23] C.M. Che, S.C. Chan, H.F. Xiang, M.C.W. Chan, Y. Liu, Y. Wang, Chem. Commun. (2004) 1484–1485.
[24] Y.Y. Lin, S.C. Chan, M.C.W. Chan, Y.J. Hou, N. Zhu, C.M. Che, Y. Liu, Y. Wang, Chem. Eur. J. 9 (2003) 1263–1272.
[25] W. Li, Z.W. Li, L.C. Li, D.Z. Liao, Z.H. Jiang, J. Solid State Chem. 180 (2007) 2973–2977.
[26] W.B. Sun, P.F. Yan, G.M. Li, H. Xu, J.W. Zhang, J. Solid State Chem. 182 (2009) 381–388.
[27] T.Z. Yu, K. Zhang, Y.L. Zhao, C.H. Yang, H. Zhang, L. Qian, D.W. Fan, W.K. Dong, L.L. Chen, Y.Q. Qiu, Inorg. Chim. Acta 361 (2008) 233–240.
[28] R. Hesse, Acta Crystallogr. 1 (1948) 200–207.
[29] H. Lipson, Acta Crystallogr. 2 (1949) 43–45.
[30] Y. Wang, Z.Y. Yang, Transition Met. Chem. 30 (2005) 902–906.
[31] M.A. Torzilli, S. Colquhoun, J. Kim, R.H. Beer, Polyhedron 21 (2002) 705–713.
[32] T.Z. Yu, K. Zhang, Y.L. Zhao, C.H. Yang, H. Zhang, D.W. Fan, W.K. Dong, Inorg. Chem. Commun. 10 (2007) 401–403.